An efficient and energy stable scheme for a phase-field model for the moving contact line problem

Sebastian Aland[1] and Feng Chen[2,*,†]

[1]*Institut für Wissenschaftliches Rechnen, TU Dresden, 01062 Dresden, Germany*
[2]*Department of Mathematics, Baruch College (CUNY), New York, NY 10010, USA*

SUMMARY

In this paper, we propose for the first time a linearly coupled, energy stable scheme for the Navier–Stokes–Cahn–Hilliard system with generalized Navier boundary condition. We rigorously prove the unconditional energy stability for the proposed time discretization as well as for a fully discrete finite element scheme. Using numerical tests, we verify the accuracy, confirm the decreasing property of the discrete energy, and demonstrate the effectiveness of our method through numerical simulations in both 2-D and 3-D. Copyright © 2015 John Wiley & Sons, Ltd.

1. INTRODUCTION

To model and simulate the dynamics of the moving contact line, where a fluid-fluid interface intersects the solid wall, is a classic and challenging problem in hydrodynamics. Traditional models of multiphase flows use the no-slip boundary condition, leading to a nonphysical singularity in the vicinity of the contact line, because the force needed to move a contact line is infinite. One way to regularize the problem is the diffuse interface method, which allows for contact line motion without slip. It has been shown that diffuse interface methods can compete quantitatively with sharp interface methods, for example, level-set or volume-of-fluid methods [1]. In the context of contact line problems, the no-slip diffuse interface method has been successfully applied to numerous problems [2–5]. However, molecular dynamics simulations have shown that in many practical cases nearly complete slip happens near the moving contact line.

To overcome this discrepancy, in [6], the authors proposed a diffuse-interface approach based on an energetic variational principle that accounts for slip at the solid boundary. Their method couples a Cahn–Hilliard equation with dynamic contact angle boundary condition with a Navier–Stokes equation with generalized Navier boundary condition (GNBC). The approach can produce consistent results with molecular dynamics simulation and has recently drawn a lot of attention from researchers in computational fluid dynamics (cf. [7–9]). It is also noted that similar boundary conditions have been proposed in [10]. The design of efficient and robust numerical methods for this nonlinear, coupled system with complex boundary conditions still poses a great challenge and is the focus of this paper.

Though efficient numerical schemes for Cahn–Hilliard equations and Navier–Stokes equations have been established in separate with many approaches (cf. [11–16]), a direct combination of the

---

*Correspondence to: Feng Chen, Department of Mathematics, Baruch College (CUNY), New York, NY 10010, USA.
†E-mail: feng.chen@baruch.cuny.edu

two does not necessarily yield a successful scheme. The strong coupling both in the system and the boundary conditions calls for novel techniques in terms of temporal and spatial discretization. In [17], an operator splitting scheme in time and a least-squares/finite element method in space was used. The authors showed conditional energy stability (for a mild time steps restriction) of the temporal discretization scheme. In [18], the authors developed energy stable temporal schemes and discretized the system with a staggered grid finite difference method in space. In addition, they compared different effects of the pressure projection correction method and the consistent splitting method and concluded that the latter provided better performance. All the above schemes require solving nonlinear equations so that sub-iterations (e.g. CG) are needed at each time step, which limits their efficiency. A first linear and energy stable scheme was proposed in [19], where a projection method for the Navier–Stokes equation is combined with a spectral solver. Recently, the authors of [20, 21] designed an efficient time-stepping scheme involving only constant coefficient matrices and verified a velocity projection correction method for the system, though a rigorous stability proof was not provided. Fully discrete energy stable schemes, that carry over the energy stability to the space discretization have not been proposed so far.

The major objective of this paper is to design efficient, linear, energy stable schemes for the Cahn–Hilliard–Navier–Stokes system with GNBC. The key lies in a delicate treatment of the elastic stress in the Navier–Stokes equation and the advection term in the Cahn–Hilliard equation as well as their boundary conditions. In order to achieve energy stability, the advection velocity and the chemical potential should be treated implicitly. Meanwhile, the gradient of the phase-field should be treated explicitly to yield a linear scheme. Though the aforementioned treatment is not new for no-slip models (cf. [22, 23]), the idea does not seem fulfilled in most of existing stable schemes.

Based on an energy stable scheme for the Cahn–Hilliard equation, a semi-implicit scheme for the Navier–Stokes equation and proper treatments for the interaction terms, we propose in this paper for the first time a linear, fully discrete, energy stable scheme for the Cahn–Hilliard–Navier–Stokes with GNBC. We provide a rigorous proof for the energy stability of the temporal scheme as well as for the fully discrete finite element method. We report the order of accuracy as well as the energy stability of the proposed method and demonstrate numerical results consistent with previous literature. Moreover, we provide a 3-D numerical experiments of the phase-field model for the moving contact line problem.

The paper is organized as follows. Details of the governing system and the continuous energy law are described in Section 2. They are important for an in-depth discussion in Section 3, for the temporal discretization. In Section 4, we describe the spatial discretization. Section 5 is dedicated to various numerical results. We end the paper with concluding remarks in the final section.

2. A PHASE-FIELD MODEL FOR THE MOVING CONTACT LINE PROBLEM

Let Ω be an open subset of $\mathbb{R}^2$ or $\mathbb{R}^3$. We consider the following coupled system of an elastic Navier–Stokes equation with the generalized Navier boundary condition [17],

$$\mathcal{R}\left(\boldsymbol{v}_t + \boldsymbol{v}\cdot\nabla\boldsymbol{v}\right) = \nabla\cdot\boldsymbol{\sigma} - \nabla p + \mathcal{B}\mu\nabla\phi, \qquad \text{in } \Omega, \qquad (2.1a)$$

$$\nabla\cdot\boldsymbol{v} = 0, \qquad \text{in } \Omega, \qquad (2.1b)$$

$$\boldsymbol{v}\cdot\boldsymbol{n} = 0, \qquad \text{on } \partial\Omega, \qquad (2.1c)$$

$$[\boldsymbol{\sigma}\boldsymbol{n} + l(\phi)\boldsymbol{v}_s - \mathcal{B}L(\phi)\nabla\phi]\times\boldsymbol{n} = 0, \qquad \text{on } \partial\Omega. \qquad (2.1d)$$

and an advected Cahn–Hilliard equation with the dynamic contact angle boundary condition,

$$\phi_t + \boldsymbol{v}\cdot\nabla\phi = M\Delta\mu, \qquad \text{in } \Omega, \qquad (2.2a)$$

$$\mu = -\epsilon\Delta\phi + f(\phi), \qquad \text{in } \Omega, \qquad (2.2b)$$

$$\phi_t + \boldsymbol{v}\cdot\nabla\phi = -\nu L(\phi), \qquad \text{on } \partial\Omega, \qquad (2.2c)$$

$$\partial_{\boldsymbol{n}}\mu = 0, \qquad \text{on } \partial\Omega, \qquad (2.2d)$$

where $\boldsymbol{v}$ is the flow velocity field, p the flow pressure, ϕ the phase variable, μ the chemical potential, $\mathcal{R}$ the Reynolds number, M the mobility coefficient, ν the relaxation parameter, ϵ the interface width, $\boldsymbol{n}$ the outward normal of $\partial\Omega$, $\mathcal{B}$ a scaled inverse capillary number, and $l(\phi)$ describes the inverse of the slip length [18]. Noted that (2.1d) is not a traditional boundary condition, indicating the tangential part of the involved quantity is vanished. The viscous stress and the slip velocity are defined as follows,

$$\boldsymbol{\sigma} = \eta(\phi)\boldsymbol{D}\boldsymbol{v}, \tag{2.3}$$

$$\boldsymbol{v}_{\mathrm{s}} = \boldsymbol{v}_{\tan} - \boldsymbol{v}_{\mathrm{w}}, \tag{2.4}$$

where $\boldsymbol{D}\boldsymbol{v} = \nabla\boldsymbol{v} + \nabla\boldsymbol{v}^{\mathrm{T}}$ is the symmetrized gradient, I is the identity matrix, $\boldsymbol{v}_{\tan}$ is the tangential velocity along the boundary, $\boldsymbol{v}_{\mathrm{w}}$ is the wall velocity, and

$$\eta(\phi) = \frac{1}{2\eta^*}(\eta_1(1 - \phi) + \eta_2(1 + \phi)) \tag{2.5}$$

is the viscosity ratio of the two fluids with respect to the characteristic viscosity η^*.

Furthermore, $f(\phi)$ is the first derivative of a double well potential $F(\phi) = \frac{1}{4\epsilon}(1-\phi^2)^2$ and hence

$$f(\phi) = \frac{1}{\epsilon}(\phi^3 - \phi). \tag{2.6}$$

To complete the system (2.1)–(2.2), we define

$$L(\phi) = \epsilon\partial_{\boldsymbol{n}}\phi + \gamma^{prime}(\phi), \tag{2.7}$$

where the fluid–solid interfacial free energy

$$\gamma(\phi) = -\frac{\sqrt{2}}{3}\cos\theta\sin\left(\frac{\pi}{2}\phi\right), \tag{2.8}$$

was verified in [24, 25] by molecular dynamics simulations, with θ being the static contact angle between the interface and the wall.

Next, we derive the continuous energy law for (2.1)–(2.2). The total energy E_{total} of a two-phase system interacting with a solid wall can be written as

$$E_{\mathrm{total}} = \mathcal{R}E_k + \mathcal{B}E_b + \mathcal{B}E_s, \tag{2.9}$$

with

$$E_{\mathrm{k}} = \frac{1}{2}\|\boldsymbol{v}\|^2, \tag{2.10}$$

$$E_{\mathrm{b}} = (F(\phi), 1) + \frac{\epsilon}{2}\|\nabla\phi\|^2, \tag{2.11}$$

$$E_{\mathrm{s}} = \int_{\partial\Omega}\gamma(\phi)\mathrm{d}s, \tag{2.12}$$

being the kinetic energy, bulk energy, and surface energy.

Pair (2.1a) with $\boldsymbol{v}$, use integration by parts on the right hand side and (2.1b) to have

$$\mathcal{R}\frac{1}{2}\frac{\mathrm{d}}{\mathrm{d}t}\|\boldsymbol{v}\|^2 = -(\boldsymbol{\sigma}, \nabla\boldsymbol{v}) + \int_{\partial\Omega}\boldsymbol{\sigma}\boldsymbol{n}\cdot\boldsymbol{v}\mathrm{d}s + \mathcal{B}(\mu\nabla\phi, \boldsymbol{v}). \tag{2.13}$$

Notice that

$$(\boldsymbol{\sigma}, \nabla\boldsymbol{v}) = \left(\eta(\phi)(\nabla\boldsymbol{v} + \nabla\boldsymbol{v}^T), \nabla\boldsymbol{v}\right) = \frac{1}{2}\left(\eta(\phi)(\nabla\boldsymbol{v} + \nabla\boldsymbol{v}^T), \nabla\boldsymbol{v} + \nabla\boldsymbol{v}^T\right) = \int_{\Omega}\frac{\eta(\phi)}{2}|\boldsymbol{D}\boldsymbol{v}|^2\mathrm{d}x. \tag{2.14}$$

Pair (2.2a) with μ and use integration by parts on the right hand side, to have

$$(\phi_t + \boldsymbol{v} \cdot \nabla\phi, \mu) = -M \|\nabla\mu\|^2. \tag{2.15}$$

Pair (2.2b) with ϕ_t and use integration by parts on the right hand side, to have

$$(\mu, \phi_t) = \frac{\epsilon}{2} \frac{\mathrm{d}}{\mathrm{d}t} \|\nabla\phi\|^2 - \epsilon \int_{\partial\Omega} \phi_t \, \partial_{\boldsymbol{n}}\phi \mathrm{d}s + \frac{\mathrm{d}}{\mathrm{d}t}(F(\phi), 1). \tag{2.16}$$

We focus on the boundary integral in (2.16). First, using (2.7), we have

$$\epsilon \int_{\partial\Omega} \phi_t \, \partial_{\boldsymbol{n}}\phi \mathrm{d}s = \int_{\partial\Omega} \phi_t \left[L(\phi) - \gamma'(\phi) \right] \mathrm{d}s = \int_{\partial\Omega} \phi_t L(\phi) \mathrm{d}s - \frac{\mathrm{d}}{\mathrm{d}t} \int_{\partial\Omega} \gamma(\phi) \mathrm{d}s. \tag{2.17}$$

Then we use (2.2c), to have

$$\epsilon \int_{\partial\Omega} \phi_t \, \partial_{\boldsymbol{n}}\phi \mathrm{d}s = -\int_{\partial\Omega} (\boldsymbol{v} \cdot \nabla\phi + \nu L(\phi)) \, L(\phi) \mathrm{d}s - \frac{\mathrm{d}}{\mathrm{d}t} \int_{\partial\Omega} \gamma(\phi) \mathrm{d}s. \tag{2.18}$$

Simplify the aforementioned to obtain

$$\epsilon \int_{\partial\Omega} \phi_t \, \partial_{\boldsymbol{n}}\phi \mathrm{d}s = -\int_{\partial\Omega} \boldsymbol{v} \cdot \nabla\phi L(\phi) \mathrm{d}s - \nu \|L(\phi)\|_{\partial\Omega}^2 - \frac{\mathrm{d}}{\mathrm{d}t} \int_{\partial\Omega} \gamma(\phi) \mathrm{d}s. \tag{2.19}$$

Plug (2.19) into (2.16), sum up the result with (2.15) and (2.13) to have

$$\begin{aligned}
\mathcal{R}\frac{1}{2}\frac{\mathrm{d}}{\mathrm{d}t}\|\boldsymbol{v}\|^2 + \mathcal{B}\left[\frac{\mathrm{d}}{\mathrm{d}t}(F(\phi), 1) + \frac{\epsilon}{2}\frac{\mathrm{d}}{\mathrm{d}t}\|\nabla\phi\|^2 + \nu\|L(\phi)\|_{\partial\Omega}^2 + \frac{\mathrm{d}}{\mathrm{d}t}\int_{\partial\Omega}\gamma(\phi)\mathrm{d}s \right] \\
= -\int_{\Omega} \frac{\eta(\phi)}{2}|\boldsymbol{D}\boldsymbol{v}|^2\mathrm{d}x - \mathcal{B}M\|\nabla\mu\|^2 + \int_{\partial\Omega}[\boldsymbol{\sigma}\boldsymbol{n} - \mathcal{B}\nabla\phi L(\phi)] \cdot \boldsymbol{v}\mathrm{d}s.
\end{aligned} \tag{2.20}$$

With the boundary conditions (2.1c)–(2.1d), the last term in (2.20) can be rewritten:

$$\int_{\partial\Omega}[\boldsymbol{\sigma}\boldsymbol{n} - \mathcal{B}\nabla\phi L(\phi)] \cdot \boldsymbol{v}\mathrm{d}s = \int_{\partial\Omega}[\boldsymbol{\sigma}\boldsymbol{n} - \mathcal{B}\nabla\phi L(\phi)]_t \cdot \boldsymbol{v}_{\text{tan}}\mathrm{d}s = -\int_{\partial\Omega} l(\phi)\boldsymbol{v}_s \cdot \boldsymbol{v}_{\text{tan}}\mathrm{d}s. \tag{2.21}$$

With the definition of $\boldsymbol{v}_{\text{tan}}$ in (2.4), we obtain

$$\int_{\partial\Omega}[\boldsymbol{\sigma}\boldsymbol{n} - \mathcal{B}\nabla\phi L(\phi)] \cdot \boldsymbol{v}\mathrm{d}s = -\left\| l(\phi)^{\frac{1}{2}}\boldsymbol{v}_s \right\|_{\partial\Omega}^2 - \int_{\partial\Omega} l(\phi)\boldsymbol{v}_s \cdot \boldsymbol{v}_w\mathrm{d}s. \tag{2.22}$$

Therefore, we conclude with the following continuous energy law,

$$\frac{\mathrm{d}}{\mathrm{d}t}E_{\text{total}}(\boldsymbol{v}, \phi) = -\mathcal{B}M\|\nabla\mu\|^2 - \mathcal{B}\nu\|L(\phi)\|_{\partial\Omega}^2 - \int_{\Omega}\frac{\eta(\phi)}{2}|\boldsymbol{D}\boldsymbol{v}|^2\mathrm{d}x - \left\| l(\phi)^{\frac{1}{2}}\boldsymbol{v}_s \right\|_{\partial\Omega}^2 - \int_{\partial\Omega} l(\phi)\boldsymbol{v}_s \cdot \boldsymbol{v}_w\mathrm{d}s, \tag{2.23}$$

Note that the first four terms on the right-hand side of Equation (2.23) are the natural dissipations because of chemical relaxation, contact angle relaxation, viscous diffusion, and slip. The last term on the right-hand side of Equation (2.23) is the work carried out per unit time by the flow to the wall and can be positive.

3. ENERGY STABLE TIME DISCRETIZATION

In the following, we propose a first-order linear, energy stable scheme. First, we consider a common treatment for the Cahn–Hilliard equation. While the Cahn–Hilliard equation does not satisfy the maximum principle, it has been shown in [26] that for a truncated potential $F(\phi)$ with quadratic

growth at infinities, the maximum norm of the solution for the Cahn–Hilliard equation is bounded. Therefore, we truncate the double-well potential $F(\phi)$ to a C^2 function:

$$\hat{F}(\phi) = \begin{cases} \dfrac{1}{\epsilon}(|\phi| - 1)^2, & \text{if } |\phi| > 1, \\ \dfrac{1}{4\epsilon}(\phi^2 - 1)^2, & \text{else.} \end{cases} \tag{3.1}$$

Next, we present a semi-implicit Euler time discretization scheme, which is both, linear and energy stable. Suppose that $\{v^n, \phi^n\}$ are obtained from the previous time step. We solve for $\{v^{n+1}, p^{n+1}, \phi^{n+1}, \mu^{n+1}\}$ in the following system:

$$\mathcal{R}\left(\frac{v^{n+1} - v^n}{\delta t} + v^n \cdot \nabla v^{n+1}\right) = \nabla \cdot \sigma^{n+1} - \nabla p^{n+1} + \mathcal{B}\mu^{n+1}\nabla\phi^n, \qquad \text{in } \Omega, \tag{3.2a}$$

$$\nabla \cdot v^{n+1} = 0, \qquad \text{in } \Omega, \tag{3.2b}$$

$$v^{n+1} \cdot n = 0, \qquad \text{on } \partial\Omega, \tag{3.2c}$$

$$\left[\sigma^{n+1}n + l(\phi^n)v_{\text{s}}^{n+1} - \mathcal{B}\tilde{L}(\phi^{n+1})\nabla\phi^n\right] \times n = 0, \qquad \text{on } \partial\Omega, \tag{3.2d}$$

and

$$\frac{\phi^{n+1} - \phi^n}{\delta t} + v^{n+1} \cdot \nabla\phi^n = M\Delta\mu^{n+1}, \qquad \text{in } \Omega, \tag{3.3a}$$

$$\mu^{n+1} = -\epsilon\Delta\phi^{n+1} + \hat{f}(\phi^n) + \frac{s_1}{\epsilon}\left(\phi^{n+1} - \phi^n\right), \qquad \text{in } \Omega, \tag{3.3b}$$

$$\frac{\phi^{n+1} - \phi^n}{\delta t} + v^{n+1} \cdot \nabla\phi^n = -\nu\tilde{L}\left(\phi^{n+1}\right), \qquad \text{on } \partial\Omega, \tag{3.3c}$$

$$\partial_n\mu^{n+1} = 0, \qquad \text{on } \partial\Omega, \tag{3.3d}$$

where

$$\hat{f}(\phi^n) = \hat{F}'(\phi^n), \tag{3.4}$$

$$\tilde{L}(\phi^{n+1}) = \epsilon\partial_n\phi^{n+1} + \gamma'(\phi^n) + s_2\left(\phi^{n+1} - \phi^n\right) \tag{3.5}$$

$$\sigma^{n+1} = \eta(\phi^n)\boldsymbol{D}v^{n+1}. \tag{3.6}$$

Note that the additional stabilizing terms (the terms with the s_1 and s_2) are of order of the time step size δt and therefore do not affect the first order convergence of the discretized system. To choose the constants s_1 and s_2 appropriately, we introduce

$$L_1 = \max_{\phi \in \mathbb{R}} |\hat{f}'(\hat{\phi})| \leqslant \frac{2}{\epsilon}, \quad L_2 = \max_{\phi \in \mathbb{R}} |\gamma''(\hat{\phi})| \leqslant \left(\frac{\pi}{2}\right)^2 \frac{\sqrt{2}}{3}|\cos\theta|. \tag{3.7}$$

Theorem 3.1
Denote that $E_{\text{total}}^n = E_{\text{total}}(v^n, \phi^n)$. If $s_1 \geqslant L_1/2$ and $s_2 \geqslant L_2/2$, then the scheme (3.26)–(3.27) is energy stable, that is,

$$E_{\text{total}}^{n+1} - E_{\text{total}}^n + \delta t \int_{\partial\Omega} l(\phi^n)v_{\text{s}}^{n+1} \cdot v_{\text{w}}^{n+1}\text{d}s \leqslant 0, \quad n = 0, 1, 2, \cdots. \tag{3.8}$$

Proof
Taking the inner product of (3.26a) with v^{n+1}, we have

$$\frac{\mathcal{R}}{2\delta t}\left(\|v^{n+1}\|^2 - \|v^n\|^2 + \|v^{n+1} - v^n\|^2\right)$$
$$= -\int_\Omega \frac{\eta(\phi)}{2}|\boldsymbol{D}v^{n+1}|^2\text{d}x + \int_{\partial\Omega} \sigma^{n+1}n \cdot v^{n+1}\text{d}s + \mathcal{B}\left(\mu^{n+1}\nabla\phi^n, v^{n+1}\right), \tag{3.9}$$

Taking the inner product of (3.27a) with μ^{n+1}, we have

$$\left(\frac{\phi^{n+1}-\phi^n}{\delta t},\mu^{n+1}\right)+\left(\boldsymbol{v}^{n+1}\cdot\nabla\phi^n,\mu^{n+1}\right)=-M\|\nabla\mu^{n+1}\|^2. \tag{3.10}$$

Taking the inner product of (3.27b) with $(\phi^{n+1}-\phi^n)/\delta t$, we have

$$\left(\mu^{n+1},\frac{\phi^{n+1}-\phi^n}{\delta t}\right)=\frac{\epsilon}{2\delta t}\left(\|\nabla\phi^{n+1}\|^2-\|\nabla\phi^n\|^2+\|\nabla(\phi^{n+1}-\phi^n)\|^2\right)$$
$$-\epsilon\int_{\partial\Omega}\partial_{\boldsymbol{n}}\phi^{n+1}\frac{\phi^{n+1}-\phi^n}{\delta t}ds+\left(\kappa^{n+1},\frac{\phi^{n+1}-\phi^n}{\delta t}\right), \tag{3.11}$$

where

$$\kappa^{n+1}=\hat{f}(\phi^n)+\frac{s_1}{\epsilon}\left(\phi^{n+1}-\phi^n\right). \tag{3.12}$$

We focus on the boundary integral term in (3.11). Using the definition of $\tilde{L}(\phi)$, we have

$$\epsilon\int_{\partial\Omega}\partial_{\boldsymbol{n}}\phi^{n+1}\frac{\phi^{n+1}-\phi^n}{\delta t}ds=\int_{\partial\Omega}\left[\tilde{L}\left(\phi^{n+1}\right)-\gamma'(\phi^n)-s_2\left(\phi^{n+1}-\phi^n\right)\right]\frac{\phi^{n+1}-\phi^n}{\delta t}ds. \tag{3.13}$$

Simplify the aforementioned equation to be

$$\epsilon\int_{\partial\Omega}\partial_{\boldsymbol{n}}\phi^{n+1}\frac{\phi^{n+1}-\phi^n}{\delta t}ds=\int_{\partial\Omega}\tilde{L}\left(\phi^{n+1}\right)\frac{\phi^{n+1}-\phi^n}{\delta t}ds-\int_{\partial\Omega}\tau^{n+1}\frac{\phi^{n+1}-\phi^n}{\delta t}ds, \tag{3.14}$$

where

$$\tau^{n+1}=\gamma'(\phi^n)+s_2\left(\phi^{n+1}-\phi^n\right). \tag{3.15}$$

Using the boundary condition (3.27c), we obtain

$$\int_{\partial\Omega}\tilde{L}\left(\phi^{n+1}\right)\frac{\phi^{n+1}-\phi^n}{\delta t}ds=-\int_{\partial\Omega}\tilde{L}\left(\phi^{n+1}\right)\left[\boldsymbol{v}^{n+1}\cdot\nabla\phi^n+v\tilde{L}\left(\phi^{n+1}\right)\right]ds,$$
$$=-\int_{\partial\Omega}\tilde{L}\left(\phi^{n+1}\right)\nabla\phi^n\cdot\boldsymbol{v}^{n+1}ds-v\|\tilde{L}\left(\phi^{n+1}\right)\|_{\partial\Omega}^2. \tag{3.16}$$

Plug (3.16) and (3.14) into (3.11), and subtract the result from (3.10), to obtain

$$-\left(\boldsymbol{v}^{n+1}\cdot\nabla\phi^n,\mu^{n+1}\right)-\frac{\epsilon}{2\delta t}\left(\|\nabla\phi^{n+1}\|^2-\|\nabla\phi^n\|^2+\|\nabla\left(\phi^{n+1}-\phi^n\right)\|^2\right)$$
$$=\int_{\partial\Omega}\tilde{L}\left(\phi^{n+1}\right)\nabla\phi^n\cdot\boldsymbol{v}^{n+1}ds+v\|\tilde{L}\left(\phi^{n+1}\right)\|_{\partial\Omega}^2+\int_{\partial\Omega}\tau^{n+1}\frac{\phi^{n+1}-\phi^n}{\delta t}ds \tag{3.17}$$
$$+\left(\kappa^{n+1},\frac{\phi^{n+1}-\phi^n}{\delta t}\right)+M\|\nabla\mu^{n+1}\|^2.$$

Multiply (3.17) by $\mathcal{B}$ and sum up the result with (3.9), to get

$$-\frac{\mathcal{R}}{2\delta t}\left(\|\boldsymbol{v}^{n+1}\|^2-\|\boldsymbol{v}^n\|^2+\|\boldsymbol{v}^{n+1}-\boldsymbol{v}^n\|^2\right)$$
$$-\frac{\mathcal{B}\epsilon}{2\delta t}\left(\|\nabla\phi^{n+1}\|^2-\|\nabla\phi^n\|^2+\|\nabla\left(\phi^{n+1}-\phi^n\right)\|^2\right)$$
$$=\int_{\partial\Omega}\left[\mathcal{B}\tilde{L}\left(\phi^{n+1}\right)\nabla\phi^n-\boldsymbol{\sigma}^{n+1}\boldsymbol{n}\right]\cdot\boldsymbol{v}^{n+1}ds \tag{3.18}$$
$$+\mathcal{B}\int_{\partial\Omega}\tau^{n+1}\frac{\phi^{n+1}-\phi^n}{\delta t}ds+\mathcal{B}\left(\kappa^{n+1},\frac{\phi^{n+1}-\phi^n}{\delta t}\right)$$
$$+\mathcal{B}M\|\nabla\mu^{n+1}\|^2+\int_{\Omega}\frac{\eta(\phi)}{2}|\boldsymbol{D}\boldsymbol{v}^{n+1}|^2dx+\mathcal{B}v\|\tilde{L}\left(\phi^{n+1}\right)\|_{\partial\Omega}^2.$$

Now we deal with the right hand side of (3.18). With the boundary conditions of (3.26c) and (3.26d), we can rewrite the first term as

$$
\int_{\partial\Omega} \left[\mathcal{B}\tilde{L}\left(\phi^{n+1}\right)\nabla\phi^n - \sigma^{n+1}\boldsymbol{n} \right] \cdot \boldsymbol{v}^{n+1}\mathrm{d}s = \int_{\partial\Omega} \left[\mathcal{B}\tilde{L}\left(\phi^{n+1}\right)\nabla\phi^n - \sigma^{n+1}\boldsymbol{n} \right]_{\mathrm{t}} \cdot \boldsymbol{v}_{\mathrm{t}}^{n+1}\mathrm{d}s
$$
$$
= \int_{\partial\Omega} \left[l(\phi^n)\boldsymbol{v}_{\mathrm{s}}^{n+1} \right]_{\mathrm{t}} \cdot \boldsymbol{v}_{\mathrm{t}}^{n+1}\mathrm{d}s. \tag{3.19}
$$

Because $\boldsymbol{v}_{\mathrm{t}} = \boldsymbol{v}_{\mathrm{w}} + \boldsymbol{v}_{\mathrm{s}}$, we get

$$
\int_{\partial\Omega} \left[\mathcal{B}\tilde{L}(\phi^{n+1})\nabla\phi^n - \sigma^{n+1}\boldsymbol{n} \right] \cdot \boldsymbol{v}^{n+1}\mathrm{d}s = \left\| \sqrt{l(\phi^n)}\boldsymbol{v}_{\mathrm{s}}^{n+1} \right\|_{\partial\Omega}^2 + \int_{\partial\Omega} l(\phi^n)\boldsymbol{v}_{\mathrm{s}}^{n+1} \cdot \boldsymbol{v}_{\mathrm{w}}^{n+1}\mathrm{d}s. \tag{3.20}
$$

For the second term in the right side of (3.18), we use the Taylor expansion,

$$
\gamma\left(\phi^{n+1}\right) = \gamma(\phi^n) + \gamma'(\phi^n)\left(\phi^{n+1} - \phi^n\right) + \frac{\gamma''(\xi^n)}{2}\left(\phi^{n+1} - \phi^n\right)^2. \tag{3.21}
$$

Then

$$
\mathcal{B}\int_{\partial\Omega} \tau^{n+1}\frac{\phi^{n+1} - \phi^n}{\delta t}\mathrm{d}s = \frac{\mathcal{B}}{\delta t}\int_{\partial\Omega} \left[\gamma\left(\phi^{n+1}\right) - \gamma(\phi^n) + \left(s_2 - \frac{\gamma''(\xi^n)}{2} \right)\left(\phi^{n+1} - \phi^n\right)^2 \right]\mathrm{d}s. \tag{3.22}
$$

Similarly,

$$
\mathcal{B}\left(\kappa^{n+1}, \frac{\phi^{n+1} - \phi^n}{\delta t} \right) = \frac{\mathcal{B}}{\delta t}\left(\left(\hat{F}\left(\phi^{n+1}\right) - \hat{F}(\phi^n), 1 \right) + \left(\left(s_1 - \frac{f'(\chi^n)}{2} \right), \left(\phi^{n+1} - \phi^n\right)^2 \right) \right). \tag{3.23}
$$

At this end, (3.18) can be rewritten as

$$
\begin{aligned}
&\frac{\mathcal{R}}{2\delta t}\left(\|\boldsymbol{v}^{n+1}\|^2 - \|\boldsymbol{v}^n\|^2 \right) + \frac{\mathcal{B}\epsilon}{2\delta t}\left(\|\nabla\phi^{n+1}\|^2 - \|\nabla\phi^n\|^2 \right) \\
&\quad + \frac{\mathcal{B}}{\delta t}\int_{\partial\Omega} \left[\gamma\left(\phi^{n+1}\right) - \gamma(\phi^n) \right]\mathrm{d}s + \frac{\mathcal{B}}{\delta t}\left(\left(\hat{F}\left(\phi^{n+1}\right) - \hat{F}(\phi^n), 1 \right) \right) \\
&\quad + \int_{\partial\Omega} l(\phi^n)\boldsymbol{v}_{\mathrm{s}}^{n+1} \cdot \boldsymbol{v}_{\mathrm{w}}^{n+1}\mathrm{d}s = -\left\| \sqrt{l(\phi^n)}\boldsymbol{v}_{\mathrm{s}}^{n+1} \right\|_{\partial\Omega}^2 - \frac{\mathcal{R}}{2\delta t}\|\boldsymbol{v}^{n+1} \\
&\quad - \boldsymbol{v}^n\|^2 - \frac{\mathcal{B}\epsilon}{2\delta t}\|\nabla\left(\phi^{n+1} - \phi^n\right)\|^2 \\
&\quad - \mathcal{B}M\|\nabla\mu^{n+1}\|^2 - \int_\Omega \frac{\eta(\phi)}{2}|\boldsymbol{D}\boldsymbol{v}^{n+1}|^2\mathrm{d}x - \mathcal{B}\nu\|\tilde{L}\left(\phi^{n+1}\right)\|_{\partial\Omega}^2 \\
&\quad - \frac{\mathcal{B}}{\delta t}\int_{\partial\Omega} \left[\left(s_2 - \frac{\gamma''(\xi^n)}{2} \right)\left(\phi^{n+1} - \phi^n\right)^2 \right]\mathrm{d}s \\
&\quad - \frac{\mathcal{B}}{\delta t}\left(\left(s_1 - \frac{f'(\chi^n)}{2} \right), \left(\phi^{n+1} - \phi^n\right)^2 \right).
\end{aligned} \tag{3.24}
$$

The last two terms are non-positive with our assumptions on s_1 and s_2. The proof is finished. □

Remark 3.2

By assuming a first-order accuracy of the scheme, the last line in the proof of Theorem 3.1 shows that the discrete scheme recovers the energy dissipation of the continuous model (2.23) up to order of the time step size δt:

$$
\begin{aligned}
\frac{E_{\mathrm{total}}^{n+1} - E_{\mathrm{total}}^n}{\delta t} = &-\mathcal{B}M\|\nabla\mu^{n+1}\|^2 - \mathcal{B}\nu\|\tilde{L}(\phi^{n+1})\|_{\partial\Omega}^2 \\
&- \int_\Omega \frac{\eta(\phi)}{2}|\boldsymbol{D}\boldsymbol{v}^{n+1}|^2\mathrm{d}x - \left\| \sqrt{l(\phi^n)}\boldsymbol{v}_{\mathrm{s}}^{n+1} \right\|_{\partial\Omega}^2 \\
&- \int_{\partial\Omega} l(\phi^n)\boldsymbol{v}_{\mathrm{s}}^{n+1} \cdot \boldsymbol{v}_{\mathrm{w}}^{n+1}\mathrm{d}s + \mathcal{O}(\delta t).
\end{aligned} \tag{3.25}
$$

Remark 3.3
In the case that the wall speed is zero ($\boldsymbol{v}_\text{w} = \boldsymbol{0}$), there is no work carried out by the flow to the wall. Consequently, Theorem 3.1 states that the total energy decreases in time: $E^{n+1}_\text{total} - E^n_\text{total} \leqslant 0$.

Remark 3.4
It is often desired to reach more than the first order accuracy in time. For the Navier–Stokes–Cahn–Hilliard system without moving contact lines a nonlinear energy stable second–order scheme has been proposed in [27]. However, it seems challenging to define a linear, energy stable, second-order scheme for the moving contact line problem. Formally, our proposed linear scheme can be extended to the following second-order version with Backward Differentiation Formula (BDF2) and explicit extrapolations, but it is not clear how to carry over the previous stability analysis:

Suppose that $\{\boldsymbol{v}^n, \phi^n\}$ and $\{\boldsymbol{v}^{n-1}, \phi^{n-1}\}$ are obtained from the previous two time steps. We solve for $\{\boldsymbol{v}^{n+1}, p^{n+1}, \phi^{n+1}, \mu^{n+1}\}$ in the following system:

$$\mathcal{R}\left(\frac{3\boldsymbol{v}^{n+1} - 4\boldsymbol{v}^n + \boldsymbol{v}^{n-1}}{2\delta t} + \left(2\boldsymbol{v}^n - \boldsymbol{v}^{n-1}\right) \cdot \nabla\boldsymbol{v}^{n+1}\right)$$
$$= \nabla \cdot \boldsymbol{\sigma}^{n+1} - \nabla p^{n+1} + \mathcal{B}\mu^{n+1}\nabla\left(2\phi^n - \phi^{n-1}\right), \qquad \text{in } \Omega, \tag{3.26a}$$

$$\nabla \cdot \boldsymbol{v}^{n+1} = 0, \qquad \text{in } \Omega, \tag{3.26b}$$

$$\boldsymbol{v}^{n+1} \cdot \boldsymbol{n} = 0, \qquad \text{on } \partial\Omega, \tag{3.26c}$$

$$\left[\boldsymbol{\sigma}^{n+1}\boldsymbol{n} + \left(2l(\phi^n) - l\left(\phi^{n-1}\right)\right)\boldsymbol{v}^{n+1}_\text{s} - \mathcal{B}\tilde{L}\left(\phi^{n+1}\right)\nabla\left(2\phi^n - \nabla\phi^{n-1}\right)\right] \times \boldsymbol{n} = 0, \qquad \text{on } \partial\Omega, \tag{3.26d}$$

and

$$\frac{3\phi^{n+1} - 4\phi^n + \phi^{n-1}}{2\delta t} + \boldsymbol{v}^{n+1} \cdot \nabla\left(2\phi^n - \phi^{n-1}\right) = M\Delta\mu^{n+1}, \qquad \text{in } \Omega, \tag{3.27a}$$

$$\mu^{n+1} = -\epsilon\Delta\phi^{n+1} + \left(2\hat{f}(\phi^n) - \hat{f}\left(\phi^{n-1}\right)\right) + \frac{s_1}{\epsilon}\left(\phi^{n+1} - 2\phi^n + \phi^{n-1}\right), \qquad \text{in } \Omega, \tag{3.27b}$$

$$\frac{3\phi^{n+1} - 4\phi^n + \phi^{n-1}}{2\delta t} + \boldsymbol{v}^{n+1} \cdot \nabla(2\phi^n - \phi^{n-1}) = -\nu\tilde{L}(\phi^{n+1}), \qquad \text{on } \partial\Omega, \tag{3.27c}$$

$$\partial_{\boldsymbol{n}}\mu^{n+1} = 0, \qquad \text{on } \partial\Omega, \tag{3.27d}$$

where

$$\hat{f}(\phi^n) = \hat{F}'(\phi^n), \tag{3.28}$$

$$\tilde{L}(\phi^{n+1}) = \epsilon\partial_{\boldsymbol{n}}\phi^{n+1} + (2\gamma'(\phi^n) - \gamma'(\phi^{n-1})) + s_2\left(\phi^{n+1} - 2\phi^n + \phi^{n-1}\right) \tag{3.29}$$

$$\boldsymbol{\sigma}^{n+1} = (2\eta(\phi^n) - \eta(\phi^{n-1}))\boldsymbol{D}\boldsymbol{v}^{n+1}. \tag{3.30}$$

4. FULLY DISCRETE FINITE ELEMENT SCHEME

We assume $\mathcal{T}_h$ to be a regular triangulation of the domain Ω. For the pressure, we will use the finite element space of continuous, piecewise linear functions on $\mathcal{T}_h$. For the velocity $\boldsymbol{v}$, phase field ϕ and chemical potential μ, we use continuous, piecewise quadratic functions. For the velocity, these functions are additionally restricted to be zero at the boundary in normal direction. Hence, we have following three finite element spaces:

$$M_h = \left\{q \in C^0(\bar{\Omega}) \ : \ q_{|K} \in P_1(K), K \in \mathcal{T}_h\right\}, \tag{4.1}$$

$$X_h = \left\{\psi \in C^0(\bar{\Omega}) \ : \ \psi_{|K} \in P_2(K), K \in \mathcal{T}_h\right\}, \tag{4.2}$$

$$V_h = \left\{ \boldsymbol{u} \in (C^0(\bar{\Omega}))^d \; : \; (\boldsymbol{u})_{j|K} \in P_2(K), K \in \mathcal{T}_h, j = 1, \ldots, d, \boldsymbol{n} \cdot \boldsymbol{u}_{|\partial\Omega} = 0 \right\}, \quad d = 2, 3. \tag{4.3}$$

For simplicity, assume that $\eta \equiv 1$. Now, the finite element approximation of the time discretized scheme (3.26)–(3.27) reads: Find $(\boldsymbol{v}^{n+1}, p^{n+1}, \phi^{n+1}, \mu^{n+1}) \in V_h \times M_h \times X_h \times X_h$ such that for all $(\boldsymbol{u}, q, \psi, \lambda) \in V_h \times M_h \times X_h \times X_h$

$$
\begin{aligned}
&\mathcal{R}\left(\frac{\boldsymbol{v}^{n+1} - \boldsymbol{v}^n}{\delta t} + \frac{1}{2} \boldsymbol{v}^n \cdot \nabla \boldsymbol{v}^{n+1}, \boldsymbol{u} \right) - \frac{\mathcal{R}}{2} \left(\boldsymbol{v}^n \cdot \nabla \boldsymbol{u}, \boldsymbol{v}^{n+1} \right) \\
&= -\left(\boldsymbol{D} \boldsymbol{v}^{n+1}, \nabla \boldsymbol{u} \right) + \left(p^{n+1}, \nabla \cdot \boldsymbol{u} \right) + \mathcal{B} \left(\mu^{n+1} \nabla \phi^n, \boldsymbol{u} \right) \\
&\quad - \int_{\partial\Omega} l(\phi^n) \boldsymbol{v}_{\mathrm{s}}^{n+1} \cdot \boldsymbol{u} - \frac{\mathcal{B}}{\nu} \left(\frac{\phi^{n+1} - \phi^n}{\delta t} + \boldsymbol{v}^{n+1} \cdot \nabla \phi^n \right) \nabla \phi^n \cdot \boldsymbol{u} \, \mathrm{d}s
\end{aligned}
\tag{4.4}
$$

$$(\nabla \cdot \boldsymbol{v}^{n+1}, q) = 0, \tag{4.5}$$

$$\left(\frac{\phi^{n+1} - \phi^n}{\delta t} + \boldsymbol{v}^{n+1} \cdot \nabla \phi^n, \psi \right) = -M \left(\nabla \mu^{n+1}, \nabla \psi \right), \tag{4.6}$$

$$
\begin{aligned}
(\mu^{n+1}, \lambda) &= \epsilon(\nabla \phi^{n+1}, \nabla \lambda) + \left(\hat{f}(\phi^n) + \frac{s_1}{\epsilon}(\phi^{n+1} - \phi^n), \lambda \right) \\
&\quad + \int_{\partial\Omega} \frac{\phi^{n+1} - \phi^n}{\delta t \, \nu} \lambda + \frac{1}{\nu} \boldsymbol{v}^{n+1} \cdot \nabla \phi^n \lambda + \gamma'(\phi^n) \lambda + s_2(\phi^{n+1} - \phi^n) \lambda \, \mathrm{d}s.
\end{aligned}
\tag{4.7}
$$

Note that this scheme intrinsically includes the boundary conditions (3.26d), (3.27c), and (3.27d) as Robin-type conditions. In Equation (4.4), we have replaced $\tilde{L}(\phi^{n+1})$ by $-\frac{\phi^{n+1} - \phi^n}{\delta t \, \nu} - \frac{1}{\nu} \boldsymbol{v}^{n+1} \cdot \nabla \phi^n$, which holds according to Equation (3.27c). This step is necessary to obtain energy stability for the fully discrete system. An antisymmetric discretization was used for the convective part of Equation (4.4) (c.f. [28, 29]).

Theorem 4.1
Under the assumption of Theorem 3.1, the fully discrete schemes (4.4)–(4.7) is energy stable, that is,

$$E_{\mathrm{total}}^{n+1} - E_{\mathrm{total}}^n + \delta t \int_{\partial\Omega} l(\phi^n) \boldsymbol{v}_{\mathrm{s}}^{n+1} \cdot \boldsymbol{v}_{\mathrm{w}}^{n+1} \mathrm{d}s \leqslant 0, \quad n = 0, 1, 2, \cdots. \tag{4.8}$$

Proof
To show the energy stability, we take the admissible test functions

$$\boldsymbol{u} = \boldsymbol{v}^{n+1}, \qquad q = p^{n+1}, \qquad \psi = \mathcal{B}\mu^{n+1}, \qquad \lambda = -\mathcal{B}\frac{\phi^{n+1} - \phi^n}{\delta t}, \tag{4.9}$$

and add up all Equations (4.4)–(4.7) to obtain

$$
\begin{aligned}
\mathcal{R}\left(\frac{\boldsymbol{v}^{n+1} - \boldsymbol{v}^n}{\delta t}, \boldsymbol{v}^{n+1} \right) &= -\left(\boldsymbol{D}\boldsymbol{v}^{n+1}, \nabla\boldsymbol{v}^{n+1} \right) - \int_{\partial\Omega} l(\phi^n) \boldsymbol{v}_{\mathrm{s}}^{n+1} \cdot \boldsymbol{v}^{n+1} \\
&\quad - \mathcal{B}M \|\nabla\mu^{n+1}\|^2 - \frac{\mathcal{B}}{\nu} \left\| \frac{\phi^{n+1} - \phi^n}{\delta t} + \boldsymbol{v}^{n+1} \cdot \nabla\phi^n \right\|_{\partial\Omega}^2 \\
&\quad - \mathcal{B}\epsilon \left(\nabla\phi^{n+1}, \nabla\frac{\phi^{n+1} - \phi^n}{\delta t} \right) \\
&\quad - \mathcal{B}\left(\hat{f}(\phi^n) + \frac{s_1}{\epsilon}(\phi^{n+1} - \phi^n), \frac{\phi^{n+1} - \phi^n}{\delta t} \right) \\
&\quad - \mathcal{B}\int_{\partial\Omega} \gamma'(\phi^n) \frac{\phi^{n+1} - \phi^n}{\delta t} + \frac{s_2}{\delta t}(\phi^{n+1} - \phi^n)^2 \mathrm{d}s.
\end{aligned}
$$

Similar techniques as in the previous section (using Taylor expansions for $\gamma(\phi^{n+1})$ and $\hat{F}(\phi^{n+1})$) lead to the energy inequality

$$\frac{E_{\text{total}}^{n+1} - E_{\text{total}}^n}{\delta t} \leqslant -\mathcal{B}M\|\nabla\mu^{n+1}\|^2 - \frac{\mathcal{B}}{\nu}\left\|\frac{\phi^{n+1} - \phi^n}{\delta t} + \boldsymbol{v}^{n+1}\cdot\nabla\phi^n\right\|_{\partial\Omega}^2 - \int_\Omega \frac{\eta(\phi)}{2}|\boldsymbol{D}\boldsymbol{v}^{n+1}|^2\mathrm{d}x$$
$$- \left\|\sqrt{l(\phi^n)}\boldsymbol{v}_{\text{s}}^{n+1}\right\|_{\partial\Omega}^2 - \int_{\partial\Omega} l(\phi^n)\boldsymbol{v}_{\text{s}}^{n+1}\cdot\boldsymbol{v}_{\text{w}}^{n+1}\mathrm{d}s$$

for the fully discrete system. $\qquad\square$

Equations (4.4)–(4.7) pose a linear system, which can be assembled with standard finite element tools without the need for any sub-iterations. For discretization, we use the adaptive finite element toolbox AMDiS [30]. In 2D, the resulting linear systems can be solved by the unsymmetric multifrontal method (UMFPACK) [31]. The larger systems in 3D require a preconditioned iterative solver. We use an FGMRES iteration together with the preconditioner proposed in [22] for the coupled Navier–Stokes Cahn–Hilliard system.

5. NUMERICAL RESULTS

We consider a moving contact line problem in a channel flow. The problem and the parameters are taken from [17]. There is a fluid-fluid interface situated in the middle of the channel domain $\Omega = (0, 100) \times (0, 40)$. To conform with [17], we use an initial phase field

$$\phi^0 = \tanh\left(\frac{x - 50}{2\sqrt{5}}\right). \tag{5.1}$$

As in [17, 18] we use symmetric conditions for contact angle and wall velocity: $\theta = 77.6°$, $\boldsymbol{v}_w = (-0.2, 0)$ at the bottom and $\theta = 102.4°$, $\boldsymbol{v}_w = (+0.2, 0)$ at the top boundary. Noted that θ and $\boldsymbol{v}_w$ were specified only on bottom and top boundaries. Further parameters are:

$$\mathcal{R} = 0.03, \quad \mathcal{B} = 12.0, \quad \nu = 5.0, \quad l(\phi) = 0.263, \quad \eta(\phi) = 1,$$

$$s_1 = 1.0, \quad s_2 = 0.125, \quad M = 5.0, \quad \epsilon = 1.0.$$

Noted that $\eta_1 = \eta_2$ implied by $\eta(\phi) = 1$. The UMFPACK solver is employed for the 2D simulations and needs around 0.5 s to solve the coupled Navier–Stokes–Cahn–Hilliard system with a total amount of 25,000 degrees of freedom. During the evolution, the two-phase interface moves along the solid boundaries until it reaches a stationary state.

5.1. Accuracy tests

We investigate the accuracy with respect to the space and time discretization. Because no exact solution is known, we use a solution computed on the next finer grid as reference solution. Errors are measured in the normalized L^2 norm (L^2 norm divided by the square root of area of the domain).

An adaptive grid is used for all computations, with fixed grid size h along the interface and $4\sqrt{2}h$ in the region away from the interface. To test the time discretization, we use $h = 0.78$ for all computations. For the space discretization, we compare all variables at the stationary state. To make the investigations of the space discretization computationally cheaper, we use $\epsilon = 3.16$ here. Table I shows the results and suggests the first order in time and approximately the second order in space.

Next, we present the computational results in the stationary state, which is assumed at around $t = 120$. In Figure 1, we show the stationary contact line together with the velocity streamlines. Figure 2 shows the velocity profiles at the bottom and top boundary of the domain. One clearly notice a large slip at the position of the contact line, which is necessary for the solution to be stationary. Note that the results reported here match very well those reported in [17, 24].

In Figure 3, we show the total energy including the accumulated work:

Table I. Accuracy of time discretization (top) and space discretization (bottom).

δt	L^2 error in ϕ	Order	L^2 error in v	Order
8 E-03	3.81 E-06		2.11 E-06	
4 E-03	1.89 E-06	1.01	1.06 E-06	0.99
2 E-03	9.48 E-07	1.00	5.29 E-07	1.00
h				
6.25	3.83 E-05		4.19 E-04	
3.13	4.93 E-06	2.96	1.35 E-04	1.64
1.56	1.38 E-06	1.84	3.35 E-05	2.01
0.78	3.51 E-07	1.98	4.98 E-06	2.75

Shown is the error with respect to the reference solution at $t = 10$. The numbers suggest the first order in time and nearly the second order in space.
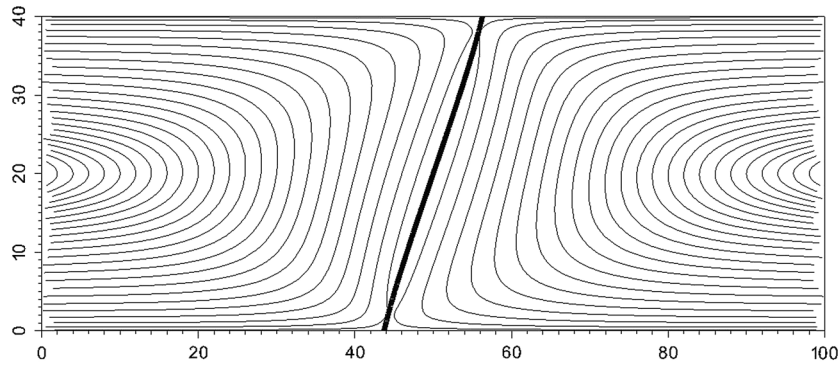
Figure 1. The stationary contact line at $t = 120$ (thick line), with streamlines illustrating flow in the bulk fluids (thin lines).
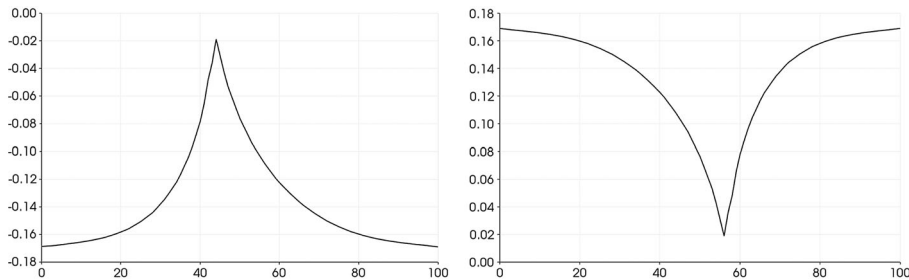
Figure 2. Velocity profiles at the stationary state at the bottom (left) and top (right) boundary of the domain. One clearly notice a large slip at the position of the contact line.

$$EW^n = E_{\text{total}}^n + \delta t \sum_{i=1}^{n} \int_{\partial\Omega} l(\phi^i) v_{\text{s}}^{i+1} \cdot v_{\text{w}}^{i+1} \mathrm{d}s. \tag{5.2}$$

From the result in Theorem 3.1, we expect this number to be non-increasing in time, which is nicely confirmed by Figure 3. Note that EW^n is still linearly decreasing in the stationary state, because work is constantly carried out. A comparison with Figure 4 from [17] shows excellent agreement. Also, we confirm that large time steps, for example, $\delta t = 1.0$, do not pose any problems for method in terms of energy stability.
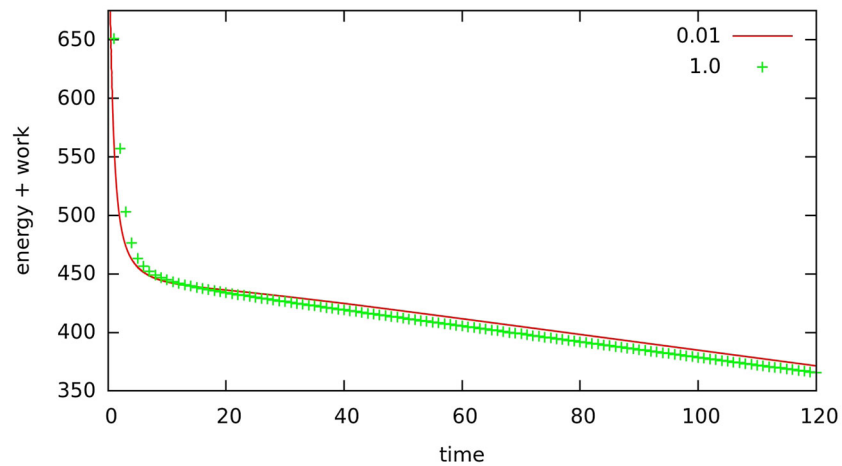
Figure 3. Total energy over time for the channel flow scenario with two different time step sizes: $\delta t = 0.01$ and $\delta t = 1.0$.
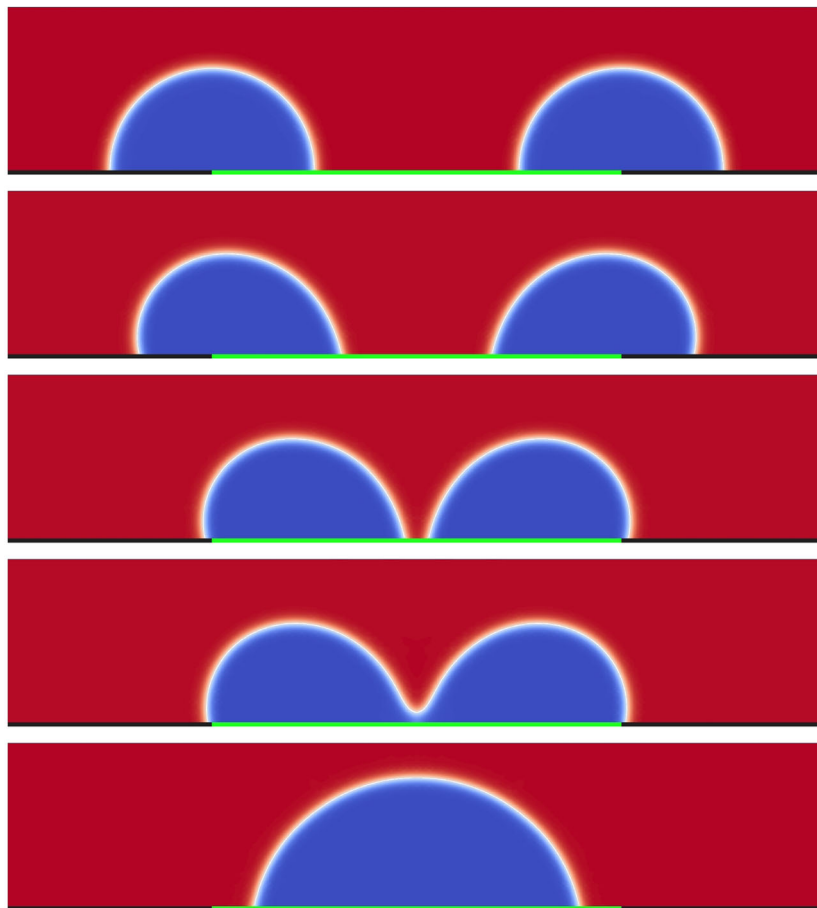

Figure 4. Two droplets on substrates with different contact angle properties. The wetting angle θ is 77.6° on the black (outer) substrate and 102.4° on the green (inner) substrate. Images are taken at $t = 0, 100, 400, 417, 700$.
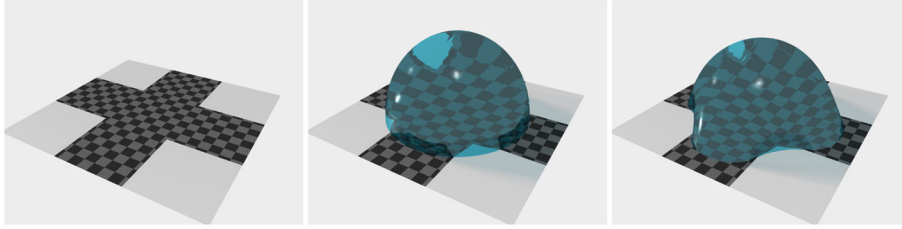
Figure 5. Droplet on substrate with different contact angle properties shown on the full domain $\Omega = (-100, 100)^2 \times (0, 100)$. The wetting angle θ is 65° on the textured part of the substrate and 115° on the plain part. Shown is the substrate (left), the initial droplet (middle) and the stationary shape (right).

5.2. Coalescing droplets

One advantage of phase field models is the capability to describe topological changes in a physically correct way. To demonstrate this property in the context of moving contact lines, we place two droplets on substrates with different contact angle properties. As initial droplets, we use two sperical caps of radius 12.5 centered at (25, 0) and (75, 0), respectively, in the domain $[0, 100] \times [0, 20]$. The wetting angle θ is 77.6° on the outer substrate and 102.4° on the inner substrate (Figure 4). We use periodic boundary conditions on the sides of the domain and the generalized Navier condition on the top and bottom wall, with zero wall velocity, $\boldsymbol{v}_w = 0$. All remaining parameters are as before. The initial velocity is zero, and the only driving force stems from contact energy between fluids and substrate. Consequently, the droplets move to the middle region, driven by the surface forces only. In this sense, they are self-propelled, targeting to minimize the contact area with the outer part of the substrate. At a certain point, both droplets coalesce. The remaining large droplet assumes a stationary shape at around $t = 700$. Figure 4 shows the time evolution of the phase field. The snapshots are taken to show the different contact angles at the front and rear of the drops as well as their state shortly before and after coalescence.

5.3. 3-D simulations

We conduct 3-D simulations to illustrate the numerical efficiency of our method. A simple drop on an inhomogeneous substrate serves as a test scenario. The substrate consists of two parts with different contact angles: 65° and 115° (Figure 5). The domain is $\Omega = (-100, 100)^2 \times (0, 100)$, as initial phase field, we prescribe a half-spherical drop of radius 70.0 in the middle of the domain. No special handling of the inhomogeneous contact angles is necessary with the current method, because γ is allowed to vary in space. To be more precise, we set the wetting angle $\theta = 65°$ for $\{(x, y, 0) \in \mathbb{R}^3 : |x| \leqslant 100/3$ or $|y| \leqslant 100/3\}$ and $\theta = 115°$ anywhere else. The parameters are as before, except for $\epsilon = 5.0, \delta t = 0.01, h = 4.16$. We use no slip boundary conditions on the sides and on the top of the domain and the generalized Navier condition on the substrate, with zero wall velocity, $\boldsymbol{v}_w = 0$. We exploit the symmetry of the problem by restricting computations to a quarter of the domain ($\Omega = (0, 100)^3$), which implies no flux conditions for ϕ and μ together with a free-slip condition for the velocity on the symmetry plane.

The preconditioned FGMRES solver is employed on a quad-core Desktop PC (2.6 GHz) to solve for approximately 180,000 degrees of freedom in each time step. The solver iterations for one time step take initially approximately 20 s and decrease to 1 s as the system keeps coming closer to the stationary state. After 700 time steps and a total computational time of 1 h, the drop is fairly close to the stationary state, which is depicted in Figure 5.

6. CONCLUSION

In this paper, an efficient and robust scheme has been proposed for the demanding problem of the Navier–Stokes–Cahn–Hilliard system with the general Navier boundary condition. It is important to treat the interaction terms properly for the coupled system as well as the coupled boundary conditions. Our method is efficient and implementation friendly, thanks to the linear coupling of the

scheme, which does not require any nonlinear sub-iterations. The discrete energy of the numerical scheme decreases unconditionally in time, indicating high reliability and robustness. This has been shown for the temporal discretization as well as for the fully discrete finite element scheme. Numerical results in both 2-D and 3-D cases were provided confirming the first order of convergence and the energy decreasing property. We thus demonstrate a practical approximation procedure for the phase-field model of the moving contact line problem. Encouraged by the good agreement of the diffuse interface methods with non-wetting two-phase flow experiments [32], we shall compare the method with experimental data in the near future.

ACKNOWLEDGEMENTS

REFERENCES

1. Aland S, Voigt A. Benchmark computations of diffuse interface models for two-dimensional bubble dynamics. *International Journal for Numerical Methods in Fluids* 2012; **69**(3):747–761.
2. Aland S, Lowengrub JS, Voigt A. Two-phase flow in complex geometries: a diffuse domain approach. *CMES-Computer Modeling in Engineering & Sciences* 2010; **57**(1):77–107.
3. Do-Quang M, Amberg G. The splash of a solid sphere impacting on a liquid surface: numerical simulation of the influence of wetting. *Physics of Fluids* 2009; **21**(2):022102.
4. Gránásy L, Pusztai T, Saylor D, Warren JA. Phase field theory of heterogeneous crystal nucleation. *Physical Review Letters* 2007; **98**(3):035703.
5. Villanueva W, Amberg G. Some generic capillary-driven flows. *International Journal of Multiphase Flow* 2006; **32**(9):1072–1086.
6. Qian T, Wang XP, Sheng P. A variational approach to moving contact line hydrodynamics. *Journal of Fluid Mechanics* 2006; **564**:333–360.
7. Nochetto RH, Salgado AJ, Walker SW. A diffuse interface model for electrowetting with moving contact lines. *Mathematical Models and Methods in Applied Sciences* 2013; **24**(1):1–45.
8. Shao S, Qian T. A variational model for two-phase immiscible electroosmotic flow at solid surfaces. *Communications in Computational Physics* 2012; **11**(3):831–862.
9. Yue P, Feng JJ. Can diffuse-interface models quantitatively describe moving contact lines? *The European Physical Journal Special Topics* 2011; **197**(1):37–46.
10. Fontelos M, Eck C. On a phase-field model for electrowetting. *Interfaces and Free Boundaries - Interface Free Bound* 2009; **11**(2):259–290.
11. Chen F, Shen J. Efficient energy stable schemes with spectral discretization in space for anisotropic Cahn-Hilliard systems. *Communications in Computational Physics* 2013; **13**(5):1189–1208.
12. Styles V, Kay D. Finite element approximation of a Cahn-Hilliard-Navier-stokes system. *Interfaces and Free Boundaries - Interface Free Bound* 2008; **10**(1):15–43.
13. Eyre DJ. Unconditionally gradient stable time marching the Cahn-Hilliard equation. In *Symposia BB Computational & Mathematical Models of Microstructural Evolution*, Vol. 529. MRS Online Proceedings Library, Materials Research Society: San Francisco, CA, 1998. p39.
14. Guermond JL, Minev P, Shen J. An overview of projection methods for incompressible flows. *Computer Methods in Applied Mechanics and Engineering* 2006; **195**(44):6011–6045.
15. Kay D, Welford R. Efficient numerical solution of Cahn-Hilliard-Navier-Stokes fluids in 2d. *SIAM Journal of Scientific Computing* 2007; **29**(6):2241–2257.
16. Shen J, Yang X. Numerical approximations of Allen-Cahn and Cahn-Hilliard equations. *Discrete and Continuous Dynamical Systems, Series A* 2010; **28**:1669–1691.
17. He Q, Glowinski R, Wang XP. A least-squares/finite element method for the numerical solution of the Navier-Stokes-Cahn-Hilliard system modeling the motion of the contact line. *Journal of Computational Physics* 2011; **230**(12):4991–5009.
18. Gao M, Wang XP. A gradient stable scheme for a phase field model for the moving contact line problem. *Journal of Computational Physics* 2012; **231**(4):1372–1386.
19. Shen J, Yang X, Yu H. Efficient energy stable numerical schemes for a phase field moving contact line model. *Journal of Computational Physics* 2015; **284**:617–630.
20. Dong S. On imposing dynamic contact-angle boundary conditions for wall-bounded liquid–gas flows. *Computer Methods in Applied Mechanics and Engineering* 2012; **247-248**:179–200.
21. Dong S, Shen J. A time-stepping scheme involving constant coefficient matrices for phase-field simulations of two-phase incompressible flows with large density ratios. *Journal of Computational Physics* 2012; **231**(17):5788–5804.
22. Aland S. Time integration for diffuse interface methods for two-phase flow. *Journal of Computational Physics* 2014; **262**:58–71.

23. Shen J, Yang X. A phase-field model and its numerical approximation for two-phase incompressible flows with different densities and viscosities. *SIAM Journal on Scientific Computing* 2010; **32**(3):1159.
24. Qian T, Wang XP, Sheng P. Molecular scale contact line hydrodynamics of immiscible flows. *Physical Review E* 2003; **68**(1):016306.
25. Qian T, Wang XP, Sheng P. Power-law slip profile of the moving contact line in two-phase immiscible flows. *Physical Review Letters* 2004; **93**(9):094501.
26. Caffarelli LA., Muler NE. An l^∞ bound for solutions of the Cahn-Hilliard equation. *Archive for Rational Mechanics and Analysis* 1995; **133**(2):129–144.
27. Han D, Wang X. A second order in time, uniquely solvable, unconditionally stable numerical scheme for Cahn-Hilliard-Navier-Stokes equation. *Journal of Computational Physics* 2015; **290**:139–156.
28. Grün G. On convergent schemes for diffuse interface models for two-phase flow of incompressible fluids with general mass densities. *SIAM Journal on Numerical Analysis* 2013; **51**(6):3036–3061.
29. Temam R. *Navier-Stokes Equations: Theory and Numerical Analysis,* vol. 343. Amer Mathematical Society: Providence, RI, 2001.
30. Vey S, Voigt A. Amdis: adaptive multidimensional simulations. *Computing and Visualization in Science* 2007; **10**(1):57–67.
31. Davis TA. Algorithm 832: UMFPACK V4.3—an unsymmetric-pattern multifrontal method. *ACM Transactions on Mathematical Software* 2004; **30**(2):196–199.
32. Aland S, Boden S, Hahn A, Klingbeil F, Weismann M, Weller S. Quantitative comparison of Taylor flow simulations based on sharp- and diffuse-interface models. *International Journal for Numerical Methods in Fluids* 2013; **73**: 344–361.